

Reduction of Non-Volatile Particulate Matter Emissions of a Commercial Turbofan Engine at Ground Level from the Use of a Sustainable Aviation Fuel Blend

Lukas Durdina^{a,1,*}, Benjamin T. Brem^{a,2,*}, Miriam Elser^{a,3}, David Schönenberger^{a,4}, Frithjof Siegerist^b, Julien G. Anet^c

^aAdvanced Analytical Technologies, Empa, Dübendorf, CH-8600, Switzerland

^bSR Technics Switzerland AG, Zurich-Airport, CH-8058, Switzerland

^cCentre for Aviation, School of Engineering, Zurich University of Applied Sciences, Winterthur, CH-8401, Switzerland

Abstract

Non-volatile particulate matter (nvPM) emissions from aircraft turbine engines deteriorate air quality and contribute to climate change. These emissions can be reduced by using sustainable aviation fuels (SAFs). Here, we investigate the effects of a 32% SAF blend with fossil fuel on particle size distributions and nvPM emission indices of a widely used turbofan engine. The experiments were conducted in a test cell using a standardized sampling and measurement system. The geometric mean diameter (GMD) increased with thrust from ~8 nm at idle to ~40 nm at take-off, and the geometric standard deviation (GSD) was in the range of 1.74 to 2.01. The SAF blend reduced the GMD and GSD at each test point. The nvPM emission indices were reduced most markedly at idle by 70% in terms of nvPM mass and 60% for nvPM number. The relative reduction of nvPM emissions decreased with the increasing thrust. The SAF blend reduced the nvPM emissions from the standardized landing and take-off cycle by 20% in terms of nvPM mass and 25% in terms of nvPM number. This work will help develop standardized models of fuel composition effects on nvPM emissions and evaluate the impacts of SAF on air quality and climate.

Keywords

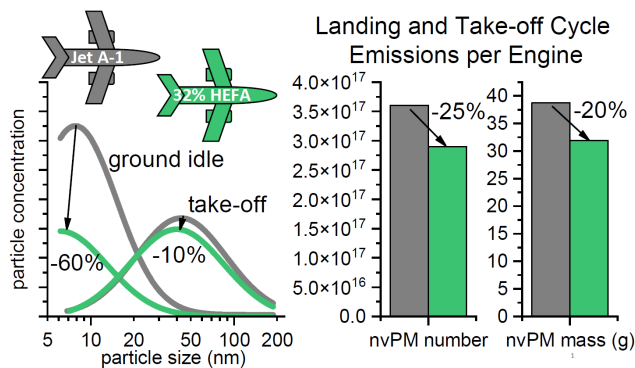
Aviation emissions, sustainable aviation fuel, particulate matter, black carbon, air pollution

Synopsis

This study evaluates air quality benefits of sustainable aviation fuels and aids to develop a standardized model for fuel composition effects on aviation PM emissions.

41 TOC art / graphical abstract

42



44 INTRODUCTION

45 The airline industry has pursued sustainable aviation fuels (SAFs) as one of the most promising
46 measures to reduce aviation's adverse effects on the environment.¹ Currently, up to 50% of
47 synthetic components made using various production pathways may be blended with
48 conventional jet fuel.² Such drop-in blends fulfill the standard specification for aviation turbine
49 fuels and can be readily used in today's aircraft without changes to operability and performance.³
50 SAF blends reduce the carbon footprint of the fuel.⁴ Due to their origin and refining, pure SAFs
51 are virtually free of sulfur and aromatic hydrocarbons.² Thus, SAF blends directly reduce
52 volatile- and non-volatile particulate matter (nvPM) emissions.⁵⁻¹⁴

53 With the prospect of increasing commercial use of SAFs, there is a growing interest in their PM
54 emissions reduction potential at the ground level and cruising altitudes. In chase studies at
55 cruising altitudes, SAF blends reduced nvPM mass and number emissions directly behind the
56 aircraft by 50 to 97% compared to conventional Jet A-1 fuel.^{10,13,15,16} Engine emission tests at
57 the ground (on-wing and in a test cell) have shown PM emissions reductions of over 90%,
58 depending on the blend ratio, engine technology, and power setting.^{5-9,11,12,14,16} The nvPM
59 emissions reduction is proportional to the decrease in soot precursors in the fuel.¹⁷ The fuel

60 composition effects on gas turbine nvPM emissions are correlated with total aromatics,
61 naphthalenes and the fuel hydrogen content. Especially the fuel hydrogen content (% mass) has
62 been used as key variable in investigations of soot formation in gas turbine combustors since
63 several decades.^{18–20} The hydrogen content accounts for the differences in the degree of
64 saturation of the aromatics (fewer ring structures in the fuel correspond to a lower number of
65 hydrogen atoms). Several recent studies have found strong correlations of nvPM and total PM
66 emissions with fuel hydrogen content.^{6,11,21–23} The fuel composition effects on nvPM depend on
67 the engine power setting. The highest reductions have been observed at low engine power (idle
68 and taxi), which has potential benefits for local air quality and health effects using SAFs.
69 ^{8,11,16,21,24}

70 As the local air quality impacts of aviation’s ultrafine PM emissions have become a growing
71 concern, the International Civil Aviation Organization’s Committee on Aviation Environmental
72 Protection (ICAO CAEP) initiated a regulatory standard for nvPM emissions.^{8,25–29} All in-
73 production engines with rated thrust F_{oo} greater than 26.7 kN have to comply with the limit for
74 the maximum nvPM mass concentration in the exhaust (CAEP/10 nvPM standard) and with the
75 limits for the nvPM mass and nvPM number emitted during the standard landing and take-off
76 (LTO) cycle normalized by F_{oo} (CAEP/11 nvPM standard).^{26,28,30} Although the nvPM
77 certification requirement is in force, there are ongoing efforts to improve the measurement
78 methodology and address uncertainty and variability sources. For example, the EU-funded
79 projects AVIATOR and RAPTOR aim to quantify measurement uncertainties and variability due
80 to instruments calibration drift, particle losses in the sampling systems, ambient conditions and
81 fuel composition.^{31,32} Despite numerous studies performed with SAFs, there is limited data
82 acquired with standardized nvPM sampling and measurement systems for large commercial

83 turbofan engines. Such data are necessary to develop a robust fuel composition effects model for
84 nvPM certification and predict the impacts on local air quality. Most previous studies of fuel
85 effects on aircraft engine PM emissions used sampling and measurement methodologies not
86 compliant with the ICAO nvPM standard.^{5,9-11,16,33} Large-scale engine testing is costly, and
87 modern engine technologies are rarely accessible. Thus, many previous fuel effects studies were
88 conducted on older technology engines, auxiliary power units (APUs), and laboratory
89 combustors, which may not represent the current commercial fleet.^{6,7,13,14,23,34,35}

90 Here, we investigate the effects of a blend of Jet A-1 with 32% of synthetic paraffinic kerosene
91 from hydrotreated esters and fatty acids (HEFA-SPK) on particle size distributions and emission
92 indices of nvPM mass (EI_{mass}) and nvPM number (EI_{num}) of the widely used CFM56-7B engine
93 (Boeing 737 family). The engine exhaust was sampled and measured using the Swiss Mobile
94 Aircraft Engine Emissions Measurement System (SMARTEMIS), one of three reference
95 sampling and measurement systems for nvPM.^{25,26} The work was done during the EMPAIREX
96 1 campaign (Emissions of Particulate and gaseous pollutants in AIRcraft engineEXhaust), and it
97 extends the work of Brem et al. 2015²¹ to thrust levels below 30% and different fuels with lower
98 levels of total aromatics.

99 **MATERIALS AND METHODS**

100 **Engine emission tests.** The engine emission tests were performed on a CFM56-7B26 engine
101 (Boeing 737NG series aircraft) in a test cell at SR Technics, Zurich airport. The engine passed all
102 performance tests for operations on commercial aircraft before and after the campaign. The
103 engine was operated on a decreasing power curve from take-off to idle. The engine test points
104 were set using the combustor inlet temperature T_3 in compliance with the ICAO emissions

105 certification procedures.³⁰ The test points chosen were based on a correlation between engine
106 thrust and T_3 at sea level determined from a calibrated engine performance model for this engine
107 type.³⁶ The test matrix contained seven test points: ground idle (~3%), 7%, 30%, 50%, 65%,
108 85%, and 100% F_{oo} ($F_{oo} = 117$ kN). The duration of each test point was from five to up to 90
109 minutes to accommodate various experiments performed during the campaign.^{24,37}

110
111 **Fuel properties.** The specifications of the fuels used are shown in Table 1. The neat Jet A-1 fuel
112 was a standard batch used at Zurich airport. The 32% HEFA-SPK blend was obtained by
113 blending the residual Jet A-1 in the test cell fuel tank with 32.6 tons of a 44.4% blend of HEFA-
114 SPK SAF supplied by SkyNRG. The neat HEFA-SPK was produced by AltAir Fuels
115 (Paramount, CA, USA; now part of World Energy) from used cooking oil. The neat SAF was
116 shipped to Europe and blended with locally stored fossil jet fuel prior to delivery to SR Technics.
117 The blend was certified to the ASTM D7566 standard for jet fuels containing synthesized
118 hydrocarbons.² The data for aromatics, naphthalene, hydrogen content, and density are averages
119 calculated from 14 samples (ten samples for Jet A-1 and four for the 32% HEFA blend). The
120 remaining parameters are based on one fuel sample of Jet A-1 and two samples of the 32%
121 HEFA blend. The analysis was performed by a certified laboratory (Intertek AG, Switzerland).
122 Additionally, the hydrogen mass content was determined in-house by nuclear magnetic
123 resonance (NMR) using a method equivalent to ASTM D7171.³⁸ The NMR-determined
124 hydrogen content was used in our analysis. For comparison with previous studies, we list the
125 hydrogen mass content determined by Intertek using the less accurate and precise method ASTM
126 D5291 for determining carbon, hydrogen, and nitrogen content (CHN).³⁹

127

128 **Table 1: Fuel properties**

Property	ASTM Method	Unit	Jet A-1	32% HEFA- SPK blend
Aromatics	D1319	vol %	18.1	11.3
Naphthalene	D1840	vol %	0.79	0.53
Hydrogen (NMR)	D7171 equivalent	mass %	13.57	14.05
Hydrogen (CHN)	D5291	mass %	13.68	14.25
H/C ratio (NMR)			1.88	1.95
Smoke point	D1322	mm	22	24
Viscosity at -20 °C	D445	mm ² /s	3.41	3.68
Specific energy	D3338	MJ/kg	43.3	43.6
Density at 15 °C	D4052	kg/m ³	795.4	781.8
Sulfur	D5453	ppm	490	350

129

130 **Exhaust sampling and measurement.** The exhaust sample was extracted < 1 m downstream of
131 the engine exit plane using a single orifice probe with an inner diameter (ID) of 8 mm made of
132 Inconel 600 alloy. The probe sampling position was checked by carbon balance (air-fuel ratio of
133 the exhaust sample agreed with the engine air-fuel ratio within 10% at all test points above idle).
134 The extracted exhaust sample was transported via a trace-heated (160°C) and insulated 5 m-long
135 stainless-steel tube with 8 mm ID to a flow splitter and diluter assembly (diluter box). At the
136 diluter box inlet, the sample was split into the pressure control line (diluter sample pressure
137 control), the nvPM transfer section, and the raw gas line. The raw gas line (160 °C, length 25 m,
138 6 mm ID, flow rate of ~18 slpm, carbon-filled poly(tetrafluoroethylene) (cPTFE)) transported the

139 raw exhaust sample to the gas and smoke analysis system (CO₂, CO, NO_x, SO₂, HC, and smoke
140 number). In the diluter box, a Dekati DI-1000 ejector diluter diluted the exhaust sample with dry
141 synthetic air by a factor of 8–11. The diluted sample was drawn through a trace-heated line (60
142 °C, length 24.2 m, 8 mm ID, flow rate of 23 slpm, cPTFE) to the PM measurement rack. In the
143 PM rack, the sample passed through a sharp cut cyclone (1 μm aerodynamic diameter cut-off)
144 and was split to various aerosol instruments and a make-up flow line with a CO₂ analyzer (Model
145 410i, Thermo Scientific). The nvPM number concentration (cut-off size d₅₀ = 10 nm) was
146 measured using an AVL Particle Counter Advanced (APC, AVL) and the nvPM mass
147 concentration was measured using an AVL Micro Soot Sensor (MSS, AVL). The MSS is a real-
148 time photoacoustic black carbon (BC) mass instrument.⁴⁰ BC mass, which is used as a surrogate
149 for nvPM mass in the regulatory standard, is calibrated to the elemental carbon (EC) mass of
150 diffusion flame soot.²⁹ The mass absorption cross-section (MAC) of the calibration aerosol used
151 by the manufacturer AVL has been found to agree with the MAC of aircraft gas turbine soot
152 within 5%.⁴¹ Diffusion flame soot calibration of the MSS has provided excellent agreement with
153 EC mass at various operating conditions of aircraft turbine engines using fossil and synthetic
154 fuels.^{37,42} The particle size distributions were measured using a fast Scanning Mobility Particle
155 Sizer (SMPS, Model 3938, TSI Inc.) operating in high flow mode (1.5 lpm nominal aerosol
156 flow), sheath to aerosol flow ratio of 12, and 30 seconds scan time. Additional aerosol
157 instruments were used to characterize effective density, chemical and optical properties, and
158 toxicity.^{24,37}

159 **Data reduction.** The emissions and engine data were averaged over three to 60 minutes during
160 stable engine operation. The averaging periods followed a stabilization period of one to three
161 minutes at each test point. Although 60-second averages are sufficient for the calculation of

162 nvPM EIs (1 Hz sampling rate), the long averaging periods provided better statistics of the
163 SMPS data.

164 The averaged data were filtered by ambient temperature to evaluate the fuel effects on nvPM
165 emissions as accurately as possible. As described above, the engine test points were set using the
166 combustor inlet temperature T_3 . At a constant T_3 , nvPM emissions can vary markedly with
167 changes in ambient temperature mainly due to the effects of varying combustor inlet pressure.²⁶
168 If emissions tests with different fuels are performed at different ambient conditions, the fuel
169 composition effects could be impossible to evaluate, especially at test points where the nvPM
170 emission characteristics vary significantly with small changes in engine operating conditions.
171 The tests with Jet A-1 were performed at ambient temperatures between 2 and 17°C and the SAF
172 blend tests between 6.5 and 12 °C. We used only data obtained with both fuels in the ambient
173 temperature range 7.5–12 °C. The nvPM EIs for all ambient conditions can be found in the
174 online supporting information (SI).

175 **Particle loss correction and size distributions.** All results are reported at the engine exit plane,
176 corrected for thermophoretic loss independent of particle size and the size-dependent particle
177 loss in the sampling and measurement system. The thermophoretic loss due to a temperature
178 gradient between the exhaust gas and the sampling line wall was calculated from the measured
179 exhaust gas temperature and the sample line temperature.³⁵ The correction factor k_{thermo} ranged
180 from 1.16 to 1.29. The size-dependent particle losses in the sampling and measurement system
181 were calculated using the particle size distributions (PSD) measured with the SMPS and modeled
182 penetration functions. The penetration functions were modeled using the system loss tool of the
183 SAE Aerospace Recommended Practice (ARP) 6481.⁴³ The penetration functions include the
184 sampling system sections from the probe inlet to the instrument inlets. The nvPM number

185 instrument has additional losses in the volatile particle remover (VPR; catalytic stripper and a
186 secondary dilution system) and due to the CPC cut-off (10 nm), which are accounted for in the
187 penetration model and are based on instrument calibration data. Since the size range of the SMPS
188 was limited to 6-190 nm, we fitted the SMPS measurement data with a product of the lognormal
189 distribution and the size-dependent penetration function. The fits were weighted by the inverse
190 squares of the standard deviations of the average PSD data. The data fitting provided the
191 number-based geometric mean diameter (GMD) and the geometric standard deviation (GSD) at
192 the engine exit plane. Due to low penetration of particles <10 nm, the measurement uncertainties
193 of these particles can be very high, and thus a lower limit of 10 nm at the engine exit plane is
194 used in the system loss correction.⁴³ The number-based nvPM correction factors were in the
195 range 2–6 (i.e., 2–6 -fold losses) and the mass-based nvPM correction factors were in the range
196 1.09–1.54 (i.e., 9–54% loss). These loss correction factors are in line with previous works that
197 calculated size-dependent losses in standardized nvPM sampling and measurement systems using
198 PSD data for various gas turbine engines.^{36,44,45} The penetration functions and the details of the
199 system loss correction calculation are in S1 of the online SI.

200 **Emission indices.** The EI_{mass} and EI_{num} were calculated using the complete EI formula, taking
201 into account the carbon monoxide (CO) and hydrocarbon (HC) gas concentrations in the exhaust
202 and the different atomic hydrogen/carbon (H/C) ratios of the two fuels.²⁹ The emission indices
203 are reported at standard temperature and pressure (STP; 0°C and 101.325 kPa). We also
204 calculated the SMPS number- and mass-based EIs for evaluating the relative reduction of nvPM
205 emissions as a function of engine thrust and fuel hydrogen content. The SMPS-based
206 concentrations were calculated by summing the number and mass concentrations in the size bins
207 (6-190 nm). The mass concentrations were calculated by assuming a constant average particle

208 density of 1 g/cm³.⁴⁶ The total standard uncertainties (95% confidence) in the EIs were estimated
209 using the root-sum-square method to propagate the uncertainties in the parameters measured as
210 described in the SAE ARP6320.²⁹ Using the typical values for systematic standard uncertainty
211 (10%) and random standard uncertainty (3%) for nvPM mass and number measurement, the total
212 standard uncertainty was 12% for EI_{mass} and 13% for EI_{num}. These uncertainties include assumed
213 2% total uncertainty for the thermophoretic loss correction factor k_{thermo} . This low uncertainty
214 agrees with recent experiments that found negligible differences between the standardized k_{thermo}
215 correction model and experimental data.³⁵ The uncertainties in the particle loss-corrected EIs
216 were calculated by propagating the total uncertainty in the EIs with the loss correction
217 uncertainties. The estimated uncertainties in the loss-corrected EIs were 22% for EI_{mass} and 26%
218 for EI_{num}. Previously, uncertainties between 20% and 38% were reported for nvPM EIs without
219 and with loss correction.^{25,26,36,44}

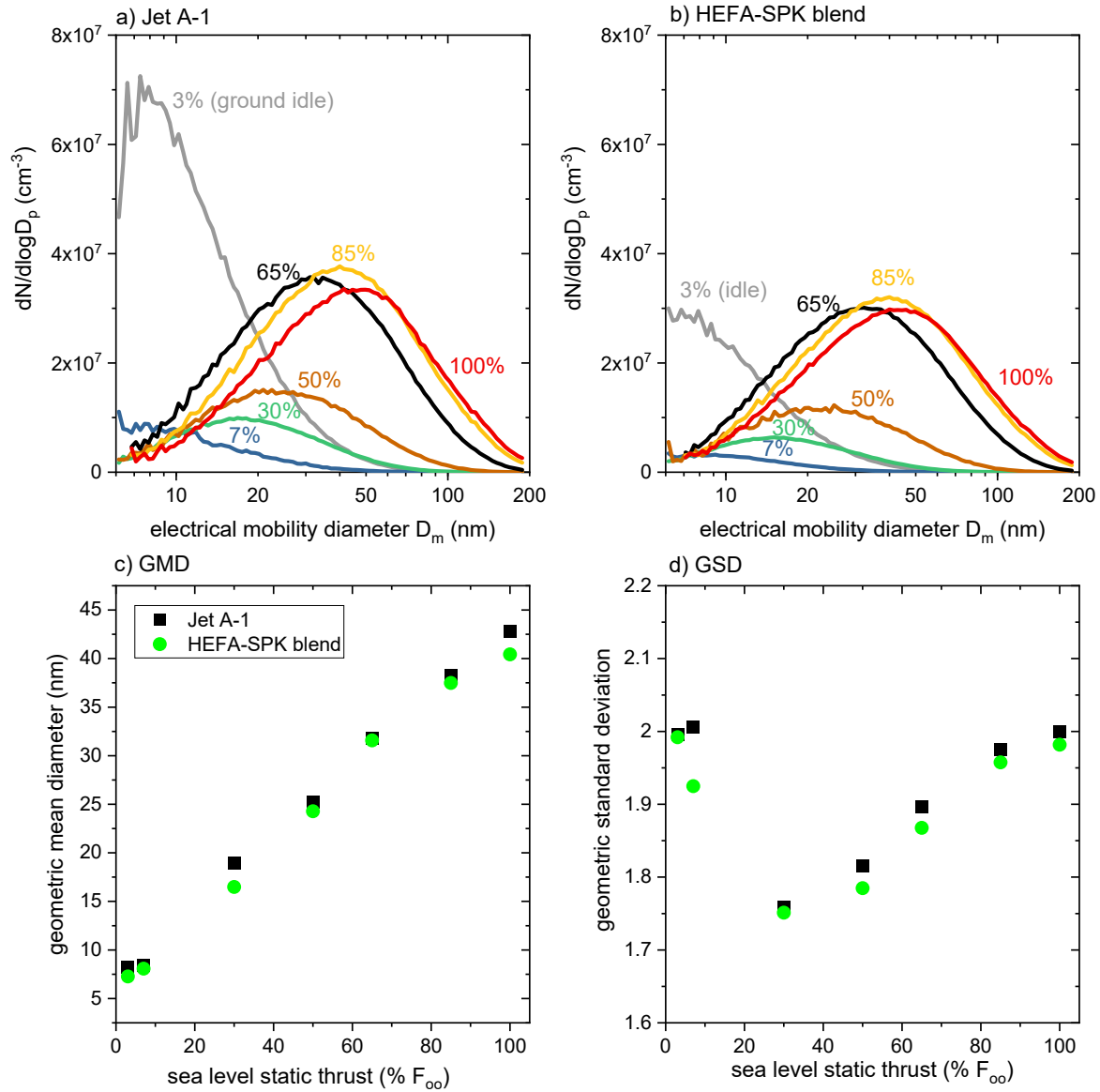
220 **LTO cycle emissions.** The average EIs and fuel flow at standard sea level (15 °C, 101.325 kPa)
221 were used to calculate emissions from the ICAO LTO cycle. The LTO cycle simulates emissions
222 from airport operations <915 m (3000 ft) above ground level. The EI in each mode is multiplied
223 by fuel flow and the mode duration (26, 4, 2.2, and 0.7 min for taxi, approach, climb-out, and
224 take-off, respectively).

225 **RESULTS AND DISCUSSION**

226 **Particle size distribution properties.** The particle size distribution properties varied with engine
227 thrust (Figure 1). At ground idle, the PSD had a GMD ~8 nm and GSD of ~2 with both fuels.
228 The PSD at ground idle with regular Jet A-1 had the highest number concentration for all test
229 points investigated (Figure 1a). When the thrust increased slightly to 7% F_{oo}, the particle number

230 concentration decreased by an order of magnitude. With further increase in thrust, the number
231 concentration increased and reached a plateau between 65% and 100% F_{oo} . The GMD increased
232 linearly with thrust and the GSD increased from 30% thrust to take-off (Figure 1, panels c and
233 d). Although the number concentration was similar at the three highest power settings, due to the
234 broadening of the PSD and increasing GMD, the mass concentration increased with thrust. The
235 PSD characteristics are in line with previous measurements of the same engine type.^{25,26,36} Note
236 that some previous studies report PSD data at the instrument, i.e. without particle loss
237 correction.^{25,26} Due to losses, size distributions at the instrument have larger GMD and lower
238 GSD than at the engine exit plane. The GMD and GSD are in the range commonly found for
239 various types of commercial turbofan engines.^{25,26,44,47}

240 The HEFA-SPK blend reduced particle concentrations in the PSD at all thrust levels (Figure 1,
241 panels a and b). The most notable reduction was observed at ground idle and 7% F_{oo} , where the
242 PSD number concentration was reduced by ~60%, and only a small reduction (10-15%) was
243 observed at high thrust. The HEFA-SPK blend reduced the GMD by up to 2.5 nm and the GSD
244 by up to 0.1. (Figure 1, panels c and d). These findings agree with previous studies done at
245 ground level and cruise with different HEFA-SPK blends, which have demonstrated relatively
246 small reductions in GMD and GSD for HEFA-SPK blends < 50%. A similar reduction of GMD
247 (~3 nm) was reported for an auxiliary power unit (APU) burning HEFA-SPK blends with Jet A-1
248 in the same range of fuel H/C ratios as investigated here (1.88–1.95).⁶ A 50% HEFA blend
249 reduced the GMD produced by a CFM56 engine at cruise by ~ 4.5 nm.¹⁰ Higher reductions in
250 GMD, by up to 30 nm, have been achieved only with higher blend ratios and pure SPK
251 fuels.^{6,12,14,23,34}

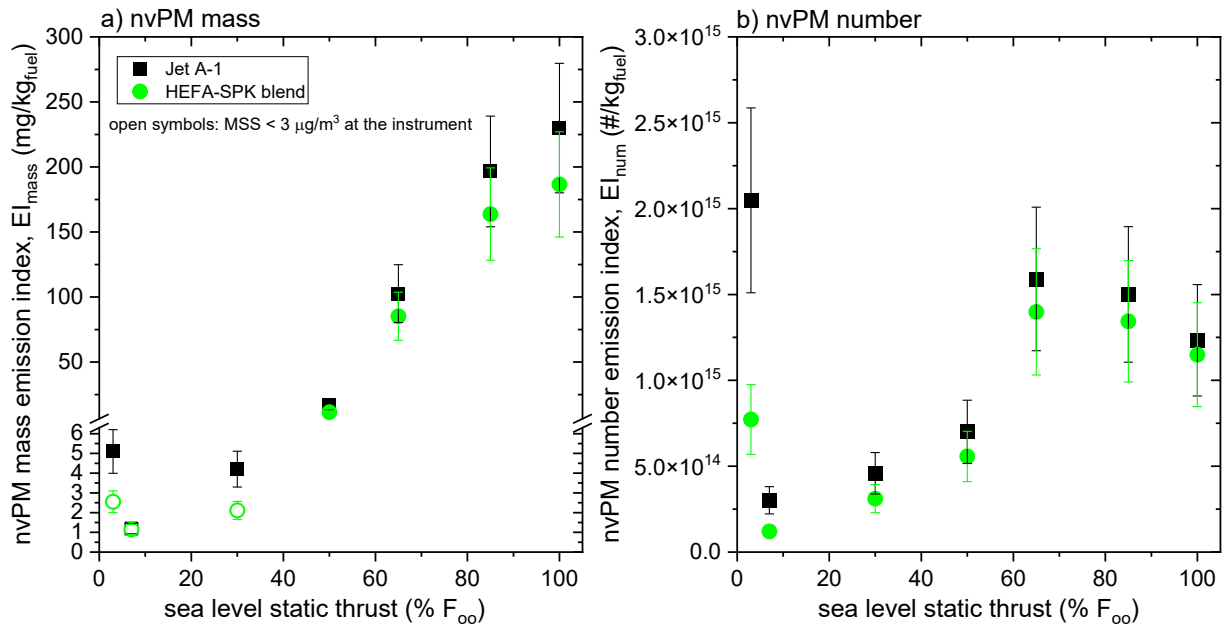


253 **Figure 1: Average particle size distributions at the engine exit plane (corrected for dilution**
 254 **and particle losses in the sampling and measurement system) at different thrust levels**
 255 **ranging from ground idle to take-off obtained with Jet-A1 (a) and the 32% HEFA-SPK**
 256 **blend (b). Panels (c) and (d) show the GMD and GSD of lognormal distributions at the**
 257 **engine exit plane obtained by fitting the SMPS measurement data with the product of the**
 258 **lognormal distribution and the sampling system penetration function ($R^2 > 0.985$; online SI).**

259 **The highest reduction in particle concentration can be seen at low thrust. A small reduction**
260 **in GMD and GSD was observed with the HEFA-SPK blend compared to the Jet A-1 fuel.**

261
262 **Emission indices of nvPM mass and number.** The nvPM EI characteristics followed the thrust
263 dependence of the particle size distribution properties. The EI_{mass} had a local maximum at ground
264 idle, then decreased to the minimum at 7% F_{oo} and subsequently increased steeply with further
265 increase in thrust (Figure 2a). The EI_{num} had a similar trend (Figure 2b). However, the maximum
266 was measured at ground idle with Jet A-1 fuel. At high thrust, the EI_{num} peaked at 65% F_{oo} and
267 decreased with further increase in thrust. The nvPM emission characteristics compare well to
268 studies of the same engine family using Jet A-1 fuel. However, the maximum EI_{mass} found here
269 was higher than reported previously.^{25,26,36} The maximum EI_{mass} was more than a factor of two
270 higher than reported for the same engine type with an improved combustor (10% lower certified
271 smoke number) burning regular Jet A-1 tested in the same facility.³⁶ In addition to the combustor
272 differences, the higher nvPM emissions can be attributed to ambient temperature effects, engine
273 deterioration, and different exhaust sampling probes. First, the data reported by Durdina et al.
274 2017³⁶ were obtained at ambient temperatures between 15°C and 34°C (compared to 7.5–12.5 °C
275 here). An engine with maximum nvPM mass emissions at full thrust produces lower EI_{mass} at the
276 T_3 corresponding to take-off at standard sea level (ISA, 15°C, 101.325 kPa) in warm conditions
277 than in cold conditions. The combustor inlet pressure p_3 and the combustor discharge fuel-air
278 ratio FAR_4 at a given T_3 decrease with increasing ambient temperature. The nvPM mass
279 reduction correlates with the decrease in p_3 and FAR_4 .^{17,48} Second, the engines tested in the
280 previous study had a lower number of flight cycles with emission performance comparable to a
281 new engine. The effects of engine aging and ambient conditions on nvPM EIs have been

282 investigated, but as of yet, no parametrizations are available. Lastly, although optimized for
 283 carbon balance, the single-orifice exhaust sampling probe used here may not capture the spatial
 284 variability of nvPM at the engine exit plane in comparison to the multi-orifice probe used
 285 previously.³⁶ For the engine type tested, the spatial variability of EI_{mass} and EI_{num} decreased with
 286 increasing thrust. At high thrust, the EI_{mass} and EI_{num} determined using the multi-orifice and
 287 single-orifice probe have been found to be within $\sim 20\%$.²⁶ However, these differences do not
 288 affect the relative nvPM emissions reductions due to fuel composition effects investigated here.



289
 290 **Figure 2: Emission indices of nvPM mass (a) and nvPM number (b) at the engine exit plane**
 291 **(corrected for particle loss in the sampling and measurement system) and STP (0°C and**
 292 **101.325 kPa). The open symbols highlight the test points with high nvPM mass**
 293 **measurement uncertainties due to low concentration at the measurement location (<3**
 294 **µg/m³ at ground idle and 30% F_{oo} and <1 µg/m³ at 7% F_{oo}). The error bars represent the 2-**
 295 **sigma (95% confidence) propagated uncertainties in the loss-corrected EIs (22% for EI_{mass}**
 296 **and 26% for EI_{num}).**

297 The $E_{I_{mass}}$ and $E_{I_{num}}$ decreased with the HEFA-SPK blend at each test point except for the $E_{I_{mass}}$
298 at 7% F_{oo} due to high measurement uncertainties at low nvPM mass concentrations (Figure 2a).
299 As highlighted by the open symbols, the nvPM mass measured at and below 30% F_{oo} with the
300 HEFA-SPK blend and at 7% F_{oo} with Jet A-1 were below $3 \mu\text{g}/\text{m}^3$ at the measurement location.
301 The lowest concentrations detected at 7% F_{oo} were below the specified limit of detection of the
302 MSS (LOD; $1 \mu\text{g}/\text{m}^3$). The reductions of nvPM emissions can be attributed to the higher
303 hydrogen mass content (+0.48%) and lower total aromatics (-6.8%) and naphthalenes (-0.26%)
304 of the HEFA-SPK blend compared to Jet A-1, which is consistent with previous research.⁵⁻
305 ^{8,11,21,23,33,45} Also, the HEFA-SPK blend had a higher smoke point, which has been historically
306 used for correlating gas turbine smoke emissions with fuels containing different amounts of total
307 aromatics, naphthalenes, and hydrogen (Table 1).¹⁸

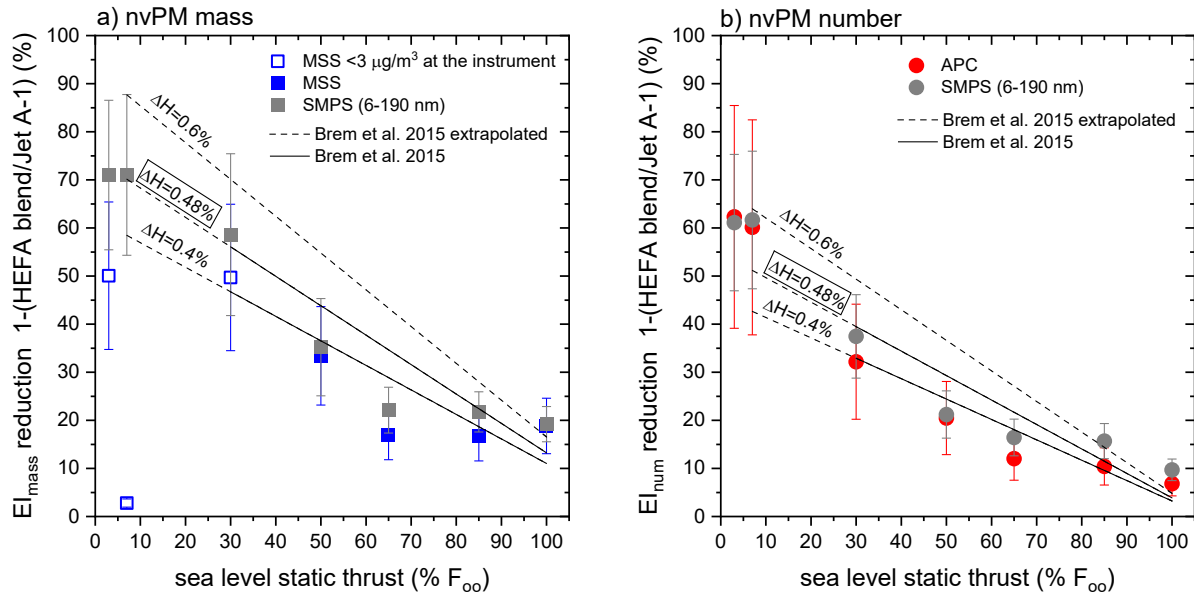
308
309 **Prediction of fuel composition effects on nvPM emissions.** This work has provided essential
310 data for developing the first standardized model of fuel composition effects used for emissions
311 certification to the new CAEP/11 nvPM standard. Studies have shown that nvPM emissions of
312 various gas turbine engine types correlate with fuel hydrogen content regardless of the
313 naphthalene and aromatics content.^{6,21,23,45} The standardized model utilizes fuel hydrogen content
314 (ΔH , difference between the hydrogen content in the fuel used and the reference value of 13.8%)
315 and engine thrust (% F_{oo}).^{28,30} The fuel composition effects are thrust dependent. Thus, the trends
316 of $E_{I_{mass}}$ and $E_{I_{num}}$ reductions with thrust (% F_{oo}) for different ΔH must be well known. In the
317 context of our study, ΔH is the difference in the hydrogen content between the two fuels
318 investigated (0.48% using the NMR-determined values in Table 1).

319

320 The EI_{mass} and EI_{num} reductions depended strongly on engine thrust setting, with the highest
321 reductions found at low thrust (Figure 3). As described above, the low thrust settings produced
322 extremely low nvPM mass concentrations ($<3 \mu\text{g}/\text{m}^3$ at the instrument). Thus, EI_{mass} reductions
323 using the MSS data at the lowest three thrust levels have very high uncertainties (open squares in
324 Figure 3a). At such low nvPM mass concentrations, the more sensitive particle size distribution
325 measurement is a useful surrogate for this analysis (gray squares and circles). The SMPS-based
326 EI_{mass} reduction was $\sim 70\%$ at ground idle and $7\% F_{\text{oo}}$. At thrust levels $>30\% F_{\text{oo}}$, the EI_{mass}
327 reductions determined using the MSS and SMPS agreed well and decreased steeply with an
328 increase in thrust, reaching $\sim 20\%$ at $65\% F_{\text{oo}}$. With a further increase in thrust, the EI_{mass}
329 reduction remained constant. At high thrust, the upper limit of the SMPS scans (190 nm) cut off
330 up to $\sim 30\%$ of the particle volume distribution, which may lead to potential discrepancies in the
331 EI_{mass} reduction predicted with the SMPS compared to the MSS. Further sources of potential
332 discrepancy between the MSS and SMPS-derived EI_{mass} reductions are changing PM chemical
333 composition (EC / total carbon (TC) ratio), MAC, and effective density with fuel composition.
334 The EC/TC ratio and MAC may affect the MSS measurement, whereas the effective density
335 affects the SMPS-derived EI_{mass} . All these parameters remained the same as a function of thrust
336 using the HEFA-SPK blend compared with the Jet A-1.^{37,49}

337 The thrust dependence of the EI_{num} reduction was similar to the EI_{mass} but with lower values at
338 each thrust level (Figure 3b). At idle and $7\% F_{\text{oo}}$, the EI_{num} reduction was $\sim 60\%$, identical for the
339 APC and SMPS. The EI_{num} reduction decreased steeply with an increased thrust to $\sim 12\%$ at 65%
340 F_{oo} . In contrast to EI_{mass} reduction, the EI_{num} reduction decreased slightly with further increase in
341 thrust, reaching $\sim 7\%$ at take-off. The consistently lower EI_{num} reduction can be explained by the

342 effect of the decreasing GMD and GSD on the particle mass distribution (third power of the
 343 particle diameter). This observation is consistent with previous studies.^{8,21}



344
 345 **Figure 3: Reduction of the emission indices of nvPM mass (a) and nvPM number (b) with**
 346 **the 32% HEFA-SPK blend with respect to Jet A-1 at the engine exit plane (corrected for**
 347 **particle loss in the sampling and measurement system). The error bars represent the**
 348 **propagated 2-sigma (95% confidence) combined uncertainties in the loss-corrected EIs.**
 349 **The lines represent the predictive model for EI_{mass} and EI_{num} reduction from Brem et al.**
 350 **2015²¹, a function of % F_{oo} and the difference in the fuel hydrogen content between the two**
 351 **fuels investigated (ΔH). The ΔH of 0.48% (framed) corresponds to the value in this study.**

352
 353 The thrust dependence of fuel composition effects qualitatively agrees with previous works,
 354 which found the highest PM and nvPM emissions reductions at low power. This effect has been
 355 seen across different jet engine technologies and sizes.^{5,7,8,11,16,33,50} The interdependencies
 356 between the local equivalence ratio governing the soot formation and fuel composition for the

357 engine type investigated have been described in detail by Brem et al.²¹ At high engine power,
358 local equivalence ratios are highest and soot is formed mainly by fragmentation and
359 polymerization reactions in fuel-rich flame zones. With decreasing thrust, the local equivalence
360 ratio decreases, mixing improves, the residence time in the primary zone increases, and the soot
361 formation favors the faster condensation reactions with aromatics.⁷ A direct comparison with
362 most of the previous emission measurements using alternative fuel blends is difficult as they
363 used various sampling and measurement methodologies not compliant with the ICAO nvPM
364 standard. However, we can compare the results of this study with the model developed by Brem
365 at al. 2015²¹ who employed the same standardized sampling and measurement system and the
366 same engine type.

367 The comparison with the fuel composition effects model of Brem et al. 2015 shows notable
368 differences in the thrust-dependent reductions (Figure 3). The model predicts a linear
369 relationship between the EI reduction and % F_{oo} for a given ΔH . The model was developed from
370 emissions tests using Jet A-1 fuel doped with aromatic solvents in the thrust range 30–100% F_{oo}
371 and $\Delta H < 0.55\%$. The solid lines in Figure 3 represent the applicability range of the model,
372 whereas the dashed lines are extrapolations of the thrust range and ΔH . For illustration, we plot
373 the predicted reductions for $\Delta H = 0.4\%$, 0.48% (ΔH in this study) and 0.6% . In agreement with
374 the model, the EI_{mass} reductions were higher than EI_{num} reductions. The extrapolations below
375 30% F_{oo} predict the reduction at the lowest certified thrust level (taxi, 7% F_{oo}) within 10%.
376 However, the model does not capture the non-linear thrust dependence with nearly constant
377 EI_{mass} and EI_{num} reductions at high thrust reported here. The different thrust dependence of the
378 fuel composition effects may be due to a deteriorated emissions performance of the engine
379 tested. The engine had accumulated three times higher number of flight cycles and hours than in

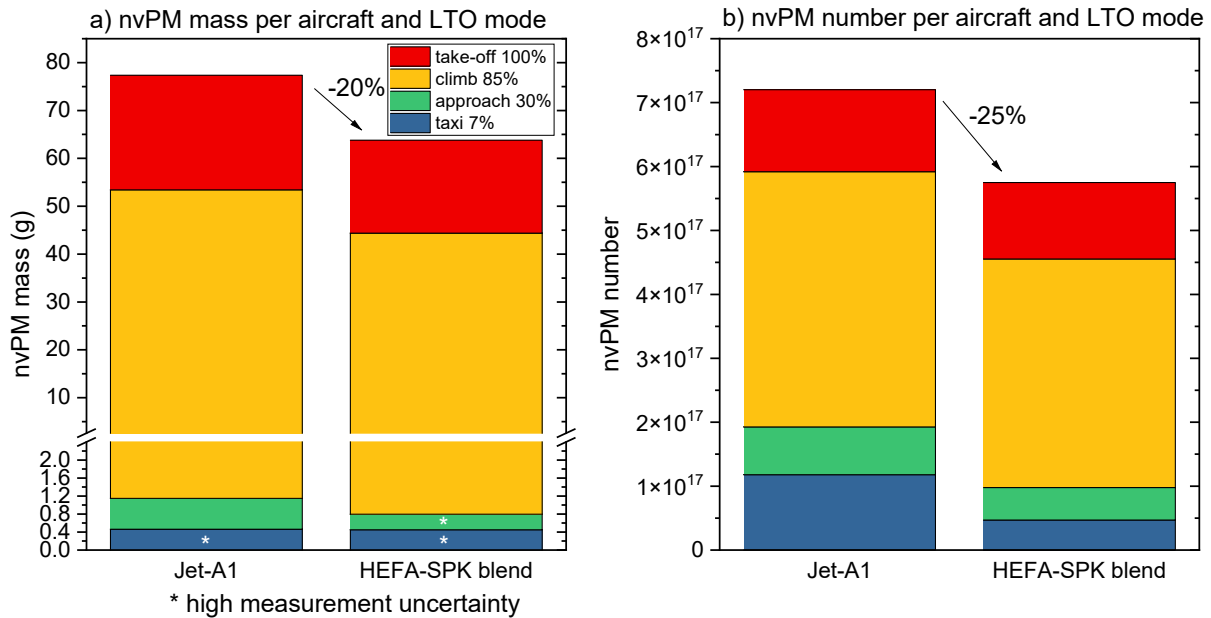
380 the previous study. Also, the engine tested by Brem et al. had an improved combustor. Using a
381 CFM56-7B engine with the same combustor as used in this study, Lobo et al.³³ reported similar
382 non-linear thrust-dependent reductions of EI_{mass} and EI_{num} (calculated from particle size
383 distributions) for various SAF/Jet A-1 blends. With each blend, the % reductions in EI_{mass} and
384 EI_{num} decreased with increasing thrust up to 85% F_{oo} and no further decrease was observed at
385 100% F_{oo} .

386 This comparison emphasizes the high uncertainties in predicting fuel composition effects on
387 nvPM emissions with published data. Future works should provide further evidence for the
388 applicability of a fuel composition correction based on fuel hydrogen content and engine thrust
389 using different SAF blends and the ICAO Annex 16 sampling and measurement methodology.
390 The tests should be performed on engines with various combustor types, thrust ratings and
391 overall pressure ratios. Accurate predictions of the fuel composition effects on nvPM emissions
392 become increasingly important for the emissions certification and predicting the impact of
393 widespread adoption of SAF on climate and local air quality.

394

395 **Local air quality impacts.** This work provides evidence of the benefits of SAF blends for
396 airport air quality. The 32% HEFA-SPK blend reduced the nvPM mass emissions from the
397 standard LTO cycle by ~20% and the nvPM number emissions by ~25% (Figure 4, no error bars
398 shown for clarity). Although we showed in Figure 3 that the EI_{mass} reductions were higher than
399 the EI_{num} reductions at each thrust level, the nvPM mass contribution to the LTO emissions from
400 the low thrust modes (where the reductions are highest) was only ~1%. In contrast, the nvPM
401 number emissions from the taxi and approach modes with Jet A-1 constituted ~25% of the LTO
402 nvPM number, leading to an overall higher reduction for the nvPM number. The overall

403 reductions were modest because the LTO emissions were dominated by climb (85% F_{00}) for both
 404 nvPM mass and nvPM number. We expect similar potential reductions of the LTO nvPM
 405 emissions from the current commercial fleet dominated by engines with maximum nvPM
 406 emissions at high thrust.



407
 408
 409 **Figure 4: Calculated emissions from the certification landing and take-off cycle (LTO) for**
 410 **nvPM mass (a) and nvPM number (b) per aircraft (2 engines operating at the same thrust).**
 411 **The different colors represent the four LTO cycle modes. The emissions in each mode are**
 412 **calculated by multiplying the EIs by fuel flow and the mode duration. The overall**
 413 **reduction is moderate because the LTO cycle emissions of this engine are dominated by the**
 414 **high thrust modes in which the nvPM emissions reductions were the lowest. The most**
 415 **significant reduction was observed for the nvPM number emissions in the taxi mode.**

416

417 The relatively high reductions of nvPM number found at low thrust are most significant for the
418 air quality and health effects at airports and surrounding communities. Recent models predict
419 that over 80% of the LTO nvPM number at a large airport is emitted during taxi and approach.⁵¹
420 However, the real-world contribution of low thrust operations may be even higher because of
421 ground idle emissions ($< 7\% F_{oo}$). As shown above, the EI_{num} at ground idle was an order of
422 magnitude higher than at $7\% F_{oo}$. Estimating real-world ground idle emissions is a point of
423 controversy as it is not a certification test point and it is set automatically by the engine control
424 unit. Moreover, in real-world operations, bleed air extraction and additional loads affect the fuel-
425 air ratio. Thus, the real-world ground idle emissions may differ from test cell results.⁵²
426 Nevertheless, we expect the relative nvPM emissions reductions found here at ground idle to
427 apply for on-wing operations. Future work should further investigate the reductions of nvPM and
428 volatile PM emissions at low power from on-wing tests at different bleed air extraction levels,
429 auxiliary loads, and ambient conditions.

430

431 **ASSOCIATED CONTENT**

432 Supporting Information. System loss correction factors, Tables with data.

433

434 **AUTHOR INFORMATION**

435 **Corresponding Authors**

436 *L.D. Email: lukas.durdina@zhaw.ch

437

438 *B.T.B. Email: benjamin.brem@psi.ch

439

440

441 **Present address**

442 ¹L.D.: Centre for Aviation, School of Engineering, Zurich University of Applied Sciences,
443 Winterthur, CH-8401, Switzerland

444 ²B.T.B.: Laboratory for Atmospheric Chemistry, Paul Scherrer Institute, Villigen, CH-5232
445 Switzerland

446 ³M.E.: Laboratory for Automotive Powertrain Technologies, Empa, Dübendorf, CH-8600,
447 Switzerland

448 ⁴D.S.: Laboratory for Air Pollution and Environmental Technology, Empa, Dübendorf, CH-
449 8600, Switzerland

450 **Notes**

451 The authors declare no competing financial interest.

452 **ACKNOWLEDGEMENTS**

453 We are grateful to SR Technics for their support regarding engine lease and the engine and test
454 cell operation. We thank Christian Bach and Martin Oertig of Empa for the help with the
455 alternative fuel blend import. We thank Dr. Daniel Rentsch and Regula Haag of Empa for the
456 NMR fuel hydrogen content analysis. Thanks to Dr. Prem Lobo for helpful comments. This work
457 was made possible by funding from the Swiss Federal Office of Civil Aviation (FOCA) through
458 projects EMPAIREX (SFLV 2015-113), AGEAIR (SFLV 2017-030) and AGEAIR 2 (SFLV
459 2018-048).

460

461 **References**

462 (1) ICAO Secretariat. Introduction to the ICAO Basket of Measures to Mitigate Climate Change. *ICAO 2019*
463 *Environmental Report*, 111–115.

464 (2) ASTM D7566-20B, *Specification for Aviation Turbine Fuel Containing Synthesized Hydrocarbons*; ASTM
465 International: West Conshohocken, PA (D7566-20B).

466 (3) ASTM D1655-20C, *Specification for Aviation Turbine Fuels*; ASTM International: West Conshohocken, PA
467 (D1655-20C).

468 (4) Staples, M. D.; Malina, R.; Suresh, P.; Hileman, J. I.; Barrett, S. R. Aviation CO₂ emissions reductions from the
469 use of alternative jet fuels. *Energ. Policy* **2018**, *114*, 342–354.

470 (5) Beyersdorf, A. J.; Timko, M. T.; Ziemba, L. D.; Bulzan, D.; Corporan, E.; Herndon, S. C.; Howard, R.; Miake-
471 Lye, R.; Thornhill, K. L.; Winstead, E.; Wey, C.; Yu, Z.; Anderson, B. E. Reductions in aircraft particulate emissions
472 due to the use of Fischer–Tropsch fuels. *Atmos. Chem. Phys.* **2014**, *14*, 11–23.

473 (6) Christie, S.; Lobo, P.; Lee, D.; Raper, D. Gas Turbine Engine Nonvolatile Particulate Matter Mass Emissions:
474 Correlation with Smoke Number for Conventional and Alternative Fuel Blends. *Environ. Sci. Technol.* **2017**, *51*,
475 988–996.

476 (7) Corporan, E.; DeWitt, M. J.; Belovich, V.; Pawlik, R.; Lynch, A. C.; Gord, J. R.; Meyer, T. R. Emissions
477 Characteristics of a Turbine Engine and Research Combustor Burning a Fischer–Tropsch Jet Fuel. *Energ. Fuel.*
478 **2007**, *21*, 2615–2626.

479 (8) Lobo, P.; Condevaux, J.; Yu, Z.; Kuhlmann, J.; Hagen, D. E.; Miake-Lye, R. C.; Whitefield, P. D.; Raper, D. W.
480 Demonstration of a Regulatory Method for Aircraft Engine Nonvolatile PM Emissions Measurements with
481 Conventional and Isoparaffinic Kerosene fuels. *Energ. Fuel.* **2016**, *30*, 7770–7777.

482 (9) Lobo, P.; Rye, L.; Williams, P. I.; Christie, S.; Tryga-Bugajska, I.; Wilson, C. W.; Hagen, D. E.; Whitefield, P.
483 D.; Blakey, S.; Coe, H.; Raper, D.; Pourkashanian, M. Impact of alternative fuels on emissions characteristics of a
484 gas turbine engine - part 1: gaseous and particulate matter emissions. *Environ. Sci. Technol.* **2012**, *46*, 10805–10811.

485 (10) Moore, R. H.; Thornhill, K. L.; Weinzierl, B.; Sauer, D.; D’Ascoli, E.; Kim, J.; Lichtenstern, M.; Scheibe, M.;
486 Beaton, B.; Beyersdorf, A. J.; Barrick, J.; Bulzan, D.; Corr, C. A.; Crosbie, E.; Jurkat, T.; Martin, R.; Riddick, D.;
487 Shook, M.; Slover, G.; Voigt, C.; White, R.; Winstead, E.; Yasky, R.; Ziemba, L. D.; Brown, A.; Schlager, H.;
488 Anderson, B. E. Biofuel blending reduces particle emissions from aircraft engines at cruise conditions. *Nature* **2017**,
489 *543*, 411–415.

490 (11) Schripp, T.; Anderson, B.; Crosbie, E. C.; Moore, R. H.; Herrmann, F.; Oßwald, P.; Wahl, C.; Kapernaum, M.;
491 Köhler, M.; Le Clercq, P.; Rauch, B.; Eichler, P.; Mikoviny, T.; Wishaler, A. Impact of Alternative Jet Fuels on
492 Engine Exhaust Composition During the 2015 ECLIF Ground-Based Measurements Campaign. *Environ. Sci.*
493 *Technol.* **2018**, *52*, 4969–4978.

494 (12) Timko, M. T.; Yu, Z.; Onasch, T. B.; Wong, H.-W.; Miake-Lye, R. C.; Beyersdorf, A. J.; Anderson, B. E.;
495 Thornhill, K. L.; Winstead, E. L.; Corporan, E.; DeWitt, M. J.; Klingshirm, C. D.; Wey, C.; Tacina, K.; Liscinsky, D.
496 S.; Howard, R.; Bharagava, A. Particulate Emissions of Gas Turbine Engine Combustion of a Fischer–Tropsch
497 Synthetic Fuel. *Energ. Fuel.* **2010**, *24*, 5883–5896.

498 (13) Tran, S.; Brown, A.; Olfert, J. S. Comparison of Particle Number Emissions from In-Flight Aircraft Fueled
499 with Jet A1, JP-5 and an Alcohol-to-Jet Fuel Blend. *Energ. Fuel.* **2020**, *34*, 7218–7222.

500 (14) Kinsey, J. S.; Timko, M. T.; Herndon, S. C.; Wood, E. C.; Yu, Z.; Miake-Lye, R. C.; Lobo, P.; Whitefield, P.;
501 Hagen, D.; Wey, C.; Anderson, B. E.; Beyersdorf, A. J.; Hudgins, C. H.; Thornhill, K. L.; Winstead, E.; Howard, R.;
502 Bulzan, D. U.; Tacina, K. B.; Knighton, W. B. Determination of the emissions from an aircraft auxiliary power unit
503 (APU) during the Alternative Aviation Fuel Experiment (AAFEX). *J. Air Waste Manag. Assoc.* **2012**, *62*, 420–430.

504 (15) Voigt, C.; Kleine, J.; Sauer, D.; Moore, R. H.; Bräuer, T.; Le Clercq, P.; Kaufmann, S.; Scheibe, M.; Jurkat-
505 Witschas, T.; Aigner, M.; Bauder, U.; Boose, Y.; Borrmann, S.; Crosbie, E.; Diskin, S. G.; DiGangi, J.; Hahn, V.;
506 Heckl, C.; Huber, F.; Nowak, J. B.; Rapp, M.; Rauch, B.; Robinson, C.; Schripp, T.; Shook, M.; Winstead, E.;
507 Ziemba, L.; Schlager, H.; Anderson, B. E. Cleaner burning aviation fuels can reduce contrail cloudiness. *Commun.*
508 *Earth. Environ.* **2021**, *2*, 1–10.

509 (16) Moore, R. H.; Shook, M.; Beyersdorf, A.; Corr, C.; Herndon, S.; Knighton, W. B.; Miake-Lye, R.; Thornhill,
510 K. L.; Winstead, E. L.; Yu, Z.; Ziemba, L. D.; Anderson, B. E. Influence of Jet Fuel Composition on Aircraft Engine
511 Emissions: A Synthesis of Aerosol Emissions Data from the NASA APEX, AAFEX, and ACCESS Missions.
512 *Energ. Fuel.* **2015**, *29*, 2591–2600.

513 (17) Lefebvre, A. H.; Ballal, D. R. Chapter 9: Emissions. *Gas turbine combustion: Alternative fuels and emissions*,
514 3. ed.; Taylor & Francis: Boca Raton, USA; 2010; pp 359–441.

515 (18) Chin, J. S.; Lefebvre, A. H. Influence of Fuel Chemical Properties on Soot Emissions from Gas Turbine
516 Combustors. *Combust. Sci. Technol.* **1990**, *73*, 479–486.

517 (19) Bowden, T. T.; Pearson, J. H.; Wetton, R. J. The Influence of Fuel Hydrogen Content Upon Soot Formation in
518 a Model Gas Turbine Combustor. *J. Eng. Gas Turb. Power* **1984**, *106*, 789–794.

519 (20) Masters, A.; Mosier, S. A.; Nowack, C. J. Fuel property effects on USN gas turbine combustors. In *Assessment*
520 *of Alternative Aircraft Fuels*, Proceedings of a conference held at NASA Lewis Research Center Cleveland Ohio,
521 1983; pp 63–71.

522 (21) Brem, B. T.; Durdina, L.; Siegerist, F.; Beyerle, P.; Bruderer, K.; Rindlisbacher, T.; Rocci-Denis, S.; Andac,
523 M. G.; Zelina, J.; Penanhoat, O.; Wang, J. Effects of Fuel Aromatic Content on Nonvolatile Particulate Emissions of
524 an In-Production Aircraft Gas Turbine. *Environ. Sci. Technol.* **2015**, *49*, 13149–13157.

525 (22) Abrahamson, J. P.; Zelina, J.; Andac, M. G.; Vander Wal, R. L. Predictive Model Development for Aviation
526 Black Carbon Mass Emissions from Alternative and Conventional Fuels at Ground and Cruise. *Environ. Sci.*
527 *Technol.* **2016**, *50*, 12048–12055.

528 (23) Lobo, P.; Christie, S.; Khandelwal, B.; Blakey, S. G.; Raper, D. W. Evaluation of Non-volatile Particulate
529 Matter Emission Characteristics of an Aircraft Auxiliary Power Unit with Varying Alternative Jet Fuel Blend
530 Ratios. *Energ. Fuel.* **2015**, *29*, 7705–7711.

531 (24) Jonsdottir, H. R.; Delaval, M.; Leni, Z.; Keller, A.; Brem, B. T.; Siegerist, F.; Schönenberger, D.; Durdina, L.;
532 Elser, M.; Burtscher, H.; Liati, A.; Geiser, M. Non-volatile particle emissions from aircraft turbine engines at
533 ground-idle induce oxidative stress in bronchial cells. *Commun. biol.* **2019**, *2*, 90.

534 (25) Lobo, P.; Durdina, L.; Smallwood, G. J.; Rindlisbacher, T.; Siegerist, F.; Black, E. A.; Yu, Z.; Mensah, A. A.;
535 Hagen, D. E.; Mlake-Lye, R. C.; Thomson, K. A.; Brem, B. T.; Corbin, J. C.; Abegglen, M.; Sierau, B.; Whitefield,
536 P. D.; Wang, J. Measurement of Aircraft Engine Non-Volatile PM Emissions: Results of the Aviation-Particle
537 Regulatory Instrumentation Demonstration Experiment (A-PRIDE) 4 Campaign. *Aerosol Sci. Technol.* **2015**, *49*,
538 472–484.

539 (26) Lobo, P.; Durdina, L.; Brem, B. T.; Crayford, A. P.; Johnson, M. P.; Smallwood, G. J.; Siegerist, F.; Williams,
540 P. I.; Black, E. A.; Llamedo, A.; Thomson, K. A.; Trueblood, M. B.; Yu, Z.; Hagen, D. E.; Whitefield, P. D.; Mlake-
541 Lye, R. C.; Rindlisbacher, T. Comparison of standardized sampling and measurement reference systems for aircraft
542 engine non-volatile particulate matter emissions. *J. Aerosol Sci.* **2020**, *145*, 105557.

543 (27) Petzold, A.; Marsh, R.; Johnson, M.; Miller, M.; Sevcenco, Y.; Delhaye, D.; Ibrahim, A.; Williams, P.; Bauer,
544 H.; Crayford, A.; Bachalo, W. D.; Raper, D. Evaluation of methods for measuring particulate matter emissions from
545 gas turbines. *Environ. Sci. Technol.* **2011**, *45*, 3562–3568.

546 (28) Jacob, S. D.; Rindlisbacher, T. The Landing and Take-Off Particulate Matter Standards for Aircraft Gas
547 Turbine Engines. *ICAO 2019 Environmental Report* **2019**, 100–105.

548 (29) *Procedure for the Continuous Sampling and Measurement of Non-Volatile Particulate Matter Emissions from*
549 *Aircraft Turbine Engines*; SAE International: 400 Commonwealth Drive, Warrendale, PA, USA.

550 (30) *Annex 16 to the Convention on International Civil Aviation: Environmental Protection, Volume II - Aircraft*
551 *Engine Emissions*, 4th Ed.; ICAO: Montreal, CA, 2017.

552 (31) Archilla, V.; Hormigo, D.; Sánchez-García, M.; Raper, D. AVIATOR - Assessing a Viation emission Impact
553 on local Air quality at airports: TOwards Regulation. *MATEC Web Conf.* **2019**, *304*, 2023.

554 (32) Durdina, L.; Durand, E.; Spirig, C.; Edebeli, J.; Anet, J.; Crayford, A. Intercomparison of two reference
555 sampling and measurement systems for aircraft engine nonvolatile PM using a small-scale RQL combustor rig
556 burning conventional and sustainable aviation fuels. In *24th ETH-Conference on Combustion Generated*
557 *Nanoparticles*, 2021.

558 (33) Lobo, P.; Hagen, D. E.; Whitefield, P. D. Comparison of PM emissions from a commercial jet engine burning
559 conventional, biomass, and Fischer-Tropsch fuels. *Environ. Sci. Technol.* **2011**, *45*, 10744–10749.

560 (34) Cain, J.; DeWitt, M. J.; Blunck, D.; Corporan, E.; Striebich, R.; Anneken, D.; Klingshirn, C.; Roquemore, W.
561 M.; Vander Wal, R. Characterization of Gaseous and Particulate Emissions From a Turboshaft Engine Burning
562 Conventional, Alternative, and Surrogate Fuels. *Energ. Fuel.* **2013**, *27*, 2290–2302.

563 (35) Durand, E. F.; Crayford, A. P.; Johnson, M. Experimental validation of thermophoretic and bend nanoparticle
564 loss for a regulatory prescribed aircraft nvPM sampling system. *Aerosol Sci. Technol.* **2020**, *54*, 1019–1033.

565 (36) Durdina, L.; Brem, B. T.; Setyan, A.; Siegerist, F.; Rindlisbacher, T.; Wang, J. Assessment of Particle
566 Pollution from Jetliners: from Smoke Visibility to Nanoparticle Counting. *Environ. Sci. Technol.* **2017**, *51*, 3534–
567 3541.

568 (37) Elser, M.; Brem, B. T.; Durdina, L.; Schönenberger, D.; Siegerist, F.; Fischer, A.; Wang, J. Chemical
569 composition and radiative properties of nascent particulate matter emitted by an aircraft turbofan burning
570 conventional and alternative fuels. *Atmos. Chem. Phys.* **2019**, *19*, 6809–6820.

571 (38) *ASTM D7171-20, Test Method for Hydrogen Content of Middle Distillate Petroleum Products by Low-*
572 *Resolution Pulsed Nuclear Magnetic Resonance Spectroscopy*; ASTM International: West Conshohocken, PA,
573 USA.

574 (39) ASTM D5291, *Test Methods for Instrumental Determination of Carbon, Hydrogen, and Nitrogen in Petroleum*
575 *Products and Lubricants*; ASTM International: West Conshohocken, PA, USA.

576 (40) Schindler, W.; Haisch, C.; Beck, H. A.; Niessner, R.; Jacob, E.; Rothe, D. A Photoacoustic Sensor System for
577 Time Resolved Quantification of Diesel Soot Emissions. In *SAE Technical Paper Series*; SAE International 400
578 Commonwealth Drive, Warrendale, PA, United States, 2004.

579 (41) Brem, B. T.; Elser, M.; Arndt M.; Fischer, A.; Durdina, L.; Schönerberger, D. The optics-chemistry link of
580 dark matter; investigating mass absorption cross sections of soot particles from two combustion sources. In *22nd*
581 *ETH-Conference on Combustion Generated Nanoparticles*, 2018.

582 (42) Kinsey, J. S.; Giannelli, R.; Howard, R.; Hoffman, B.; Frazee, R.; Aldridge, M.; Leggett, C.; Stevens, K.;
583 Kittelson, D.; Silvis, W.; Stevens, J.; Lobo, P.; Achterberg, S.; Swanson, J.; Thomson, K.; McArthur, T.; Hagen, D.;
584 Trueblood, M.; Wolff, L.; Liscinsky, D.; Arey, R.; Cerully, K.; Miake-Lye, R.; Onasch, T.; Freedman, A.; Bachalo,
585 W.; Payne, G.; Durllicki, M. Assessment of a regulatory measurement system for the determination of the non-
586 volatile particulate matter emissions from commercial aircraft engines. *J. Aerosol Sci.* **2021**, *154*, 105734.

587 (43) *Procedure for the Calculation of Non-Volatile Particulate Matter Sampling and Measurement System Losses*
588 *and System Loss Correction Factors*; SAE International: 400 Commonwealth Drive, Warrendale, PA, USA.

589 (44) Durdina, L.; Brem, B. T.; Schönerberger, D.; Siegerist, F.; Anet, J. G.; Rindlisbacher, T. Nonvolatile
590 Particulate Matter Emissions of a Business Jet Measured at Ground Level and Estimated for Cruising Altitudes.
591 *Environ. Sci. Technol.* **2019**, *53*, 12865–12872.

592 (45) Durand, E.; Lobo, P.; Crayford, A.; Sevcenco, Y.; Christie, S. Impact of fuel hydrogen content on non-volatile
593 particulate matter emitted from an aircraft auxiliary power unit measured with standardised reference systems. *Fuel*
594 **2021**, *287*, 119637.

595 (46) Durdina, L.; Brem, B. T.; Abegglen, M.; Lobo, P.; Rindlisbacher, T.; Thomson, K. A.; Smallwood, G. J.;
596 Hagen, D. E.; Sierau, B.; Wang, J. Determination of PM mass emissions from an aircraft turbine engine using
597 particle effective density. *Atmos. Environ.* **2014**, *99*, 500–507.

598 (47) Saffaripour, M.; Thomson, K. A.; Smallwood, G. J.; Lobo, P. A review on the morphological properties of
599 non-volatile particulate matter emissions from aircraft turbine engines. *J. Aerosol Sci.* **2020**, *139*, 105467.

600 (48) Petzold, A.; Döpelheuer, A.; Brock, C. A.; Schröder, F. In situ observations and model calculations of black
601 carbon emission by aircraft at cruise altitude. *J. Geophys. Res.* **1999**, *104*, 22171–22181.

602 (49) Durdina, L.; Brem, B. T.; Elser, M.; Schönerberger, D.; Anet, J. G. *Effective density of aircraft engine PM*
603 *revisited: Effects of engine thrust, engine type, fuel, and sample conditioning*; In *European Aerosol Conference*
604 *2021*.

605 (50) Speth, R. L.; Rojo, C.; Malina, R.; Barrett, S. R. Black carbon emissions reductions from combustion of
606 alternative jet fuels. *Atmos. Environ.* **2015**, *105*, 37–42.

607 (51) Lorentz, H.; Schmidt, W.; Hellebrandt, P.; Ketzler, M.; Jakobs, H.; Janicke, U. *Einfluss eines Großflughafens*
608 *auf zeitliche und räumliche Verteilungen der Außenluftkonzentrationen von Ultrafeinstaub < 100 nm, um die*
609 *potentielle Belastung in der Nähe zu beschreiben - unter Einbeziehung weiterer Luftschadstoffe (Ruß, Stickoxide und*
610 *Feinstaub (PM_{2,5} und PM₁₀))*, 2021.

611 (52) Herndon, S. C.; Wood, E. C.; Frankli, J.; Miake-Lye, R. C.; Knighton, W. B.; Babb, M.; Nakahara, A.;
612 Reynolds, T.; Balakrishnan, H. *Measurement of gaseous HAP emissions from idling aircraft as a function of engine*
613 *and ambient conditions*; ACRP report 63; Transportation Research Board: Washington, D.C., USA, 2012.

614